Environ Monit Assess (2020) 192: 375
https://doi.org/10.1007/s10661-020-08332-z

Prediction of the karstic spring flow rates under climate change by climatic variables based on the artificial neural network: a case study of Iran

Nejat Zeydalinejad · Hamid Reza Nassery · Alireza Shakiba · Farshad Alijani

Received: 12 November 2019 / Accepted: 29 April 2020 / Published online: 16 May 2020

Abstract Few studies have evaluated the impact of climate change on groundwater resources for a region with no pumping well. Indeed, the uncertainty of pumping wells may undesirably influence the results. Therefore, a region without any pumping well was selected to assess the impact of climate change on the karstic spring flow rates. NASA Earth Exchange Global Daily Downscaled Projections (NEX-GDDP) dataset was used to extract the climatic variables for the present (1961–1990) and future (2021–2050) time periods by two Representative Concentration Pathways (RCPs), i.e., RCP4.5 and RCP8.5, in Lali region, southwest Iran. Although this dataset has been already verified, its output was evaluated for Lali region. Then, the impact of climate change on the discharge of Bibitarkhoun karstic spring was examined by the Artificial Neural Network (ANN). In this regard, if considering the daily data, ANN is not trained satisfactorily, because of the spring's lag time response to the precipitation; if monthly time step is considered, the data would not be adequate. Therefore, the average of some previous days was considered to calculate the variables. The average precipitation is 344, 329, and 324 mm/year and the average temperature is 14.18, 15.98, and 16.3 °C both for the present, future time period under RCP4.5 and future time period under RCP8.5, respectively. The network selected demonstrated no climate change impact on the average of spring discharge. However, the discharge increased by about + 8% in spring and summer and decreased by about − 7% in autumn and winter in the future time period.

Keywords NEX-GDDP · Climate change · Bibitarkhoun karstic spring · ANN

N. Zeydalinejad · H. R. Nassery (✉) · A. Shakiba · F. Alijani
Faculty of Earth Sciences, Shahid Beheshti University, Tehran, Tehran, Iran
e-mail: h-nassery@sbu.ac.ir

e-mail: hamidrezanassery@yahoo.com

Introduction

There are elaborate storylines to project the climate change for a time period (IPCC 2013). To do this, the General Circulation Models (GCMs) are used and downscaling techniques are applied to address the coarse resolution of their outputs (Wilby and Wigley 1997). Various downscaling approaches with advantages and disadvantages exist, each of which is suitable for a specific purpose (Wilby et al. 2009). Nevertheless, there exist globally downscaled climate datasets available for researchers. In other words, a quick method to achieve the downscaled climate data for a specific time period is to use the outputs of GCMs, which have been already verified by observation datasets (Trotochaud et al. 2016). These datasets are user-friendly and globally applicable.

Ford and Williams (1989) uttered that approximately one-fourth of potable water in the world is provided by karstic aquifers. In other words, they constitute a quintessential portion of the freshwater resources for myriad

parts of the world (Goldscheider and Drew 2014). Moreover, Milanovic (1981) stated that karst covers the same ratio, viz. one-fourth, of the ground surface. Additionally, 11% of the ground surface in Iran is covered by karstic formations (Nassery 1992) and these formations are the main water supply, especially in Zagros Ranges. Nevertheless, karstic aquifers are vulnerable to human activities and other factors such as contamination (Drew and Hötzl 1999). In addition, study of the response of the karstic aquifers to the climate change is of paramount importance for water management.

Notwithstanding, there are several pitfalls for modeling karstic aquifers. First, in most cases, there is not sufficient data. Second, karstic aquifers are fiendishly complex, highly non-homogeneous, and non-isotropic; moreover, the exact location and geometry of caves and major conduits are unknown, and there are different flow regimes, namely fracture, conduit, and diffuse (Ford and Williams 1989). Third, it is difficult and time-consuming to simulate the karstic aquifers using numerical models. Indeed, the physical models are intricate, need detailed calculations, and include limitations, e.g., data necessities and uncertainties related to the parameters (Sahoo et al. 2017; Sun et al. 2016). Morrissey et al. (2018) simulated the groundwater flooding in the karstic terrains of south Galway, Ireland, by a physical model using the pipe network model, LiDAR data, and satellite imagery; however, they stated that more practical and economical approaches were being investigated. Brenner et al. (2018) forecasted the groundwater level in a chalk catchment disposed to karstification in southwestern England by a physical semi-distributed model. While the groundwater levels were simulated reliably up to their 75th percentile, this is not correct in relation to their 95th percentile. Moreover, they introduced some advantages and disadvantages of various modeling approaches in the karstic terrains.

Even though numerical models have various advantages such as robustness and powerfulness, they need sufficient data and information (Bardossy 2007; Pollacco et al. 2008; Yoon et al. 2016). Indeed, a complex and non-linear relationship exists between the climatic and hydrological variables (Djurovic et al. 2015). Therefore, in recent years, the newly non-numerical models such as Artificial Neural Networks (ANN) have been adopted in simulating the karstic aquifers to address these problems.

The main purpose of this study is to simulate the long-term spring's discharge rates under climate change by ANN. Simulation of long-term groundwater level is of utmost priority to assess the impact of climate change on groundwater resources and therefore, manage them efficiently (Yoon et al. 2016).

Adiat et al. (2020) demonstrated ANN can predict water table even in the intricate aquifers with weathered and fractured basements using the geoelectric parameters. However, other black box models exist that have been employed in the karstic terrains. Pla et al. (2016) applied a geographical information system (GIS) approach by making use of the climatic variables and groundwater fluctuations data induced by anthropogenic influences. By taking into account the statistical criteria, the model was able to simulate the karstic groundwater level and recharge. The methodology included three steps: (1) developing the GIS document, (2) instituting the upper boundary conditions, and (3) computing water balance. However, this approach has not been hitherto used in different karstic aquifer systems.

Daliakopoulos et al. (2005) examined the performance of different ANNs to select the optimum architecture by comparing different types of network architectures and training algorithms for predicting the groundwater level in Messara Valley, Greece. They concluded that the ANN architecture can be considered as an important factor in simulating the groundwater level and that the usual feed-forward backpropagation with Levenberg-Marquardt (LM) training algorithm rendered the best results.

Hu et al. (2008) simulated a karstic spring's discharge using ANN for a semi-arid region in China. To model the reaction of the karstic spring to precipitation, the karstic aquifer was deemed as a non-linear input/output system, and by comparing the results with a time-lag linear model, the ANN brought about better results.

Trichakis et al. (2011) applied ANN to verify whether it can simulate the groundwater level in a karstic aquifer. They acknowledged that for a karstic aquifer, there are hydrological complexities and the pertained data also is not often available. Therefore, with the utilization of a novel non-numerical method (i.e., ANN), the issue can be tackled. Data including different climatological and hydrological variables were divided into two groups: one to train (calibrate) the network and the other to gauge its ability for simulation. Findings gave credence to the great ability of ANN to simulate the karstic aquifer.

Tapoglou et al. (2014) performed a research into the application of an ANN, a multi-layer feed-forward with

particle swarm optimization (PSO) algorithm, to predict the groundwater level under climate change in Agia, Greece. They resorted to the climatological (i.e., precipitation and temperature) and hydrological (i.e., hydraulic head of an adjacent observation well) variables as inputs and concluded that the procedure could predict the general trend of the system accurately; however, they found out that some phenomena like the abrupt water level changes induced by pumping wells could not be simulated by the network accurately. Moreover, Smiatek et al. (2013) investigated the impact of climate change on one of the largest karstic spring, Figeh spring in Syria, using a downscaled dataset of climatic variables with 25 × 25 km spatial resolution and ANN approach. Time period 1961–1990 was considered as the present time period and 2021–2050 and 2070–2099 were considered as the future time periods. Results signaled the precipitation reduction and temperature enhancement in the future time period under climate change. Finally, they corroborated that spring discharge would decline by around 20% and 50% for 2021–2050 and 2070–2099 time periods, respectively.

Like Tapoglou et al. (2014), the study by Trichakis et al. (2011) concluded that enough and accurate knowledge about the pumping wells are required to simulate the hydraulic head in the karstic aquifers, especially in relation to the abrupt changes of groundwater level. Therefore, to grapple with the problem, Bibitarkhoun karstic spring—which is the largest karstic spring in Lali area, southwest Iran, for which there are no pumping wells to affect the results—was selected. It means the present paper deals with a climate change study without the uncertainty of pumping wells.

Bao and Wen (2017) applied NASA Earth Exchange Global Daily Downscaled Projections (NEX-GDDP) dataset to project the near- and long-term future climate in China by representing this dataset as a new daily downscaled dataset with extremely high resolution and complete data that reduces the biases of GCMs and has the potential to be widely used in the future. Daksiya et al. (2017) investigated the maximum daily precipitation for Jakarta, Indonesia, in the future time period using three downscaling techniques, including LARS-WG, SDSM, and NEX-GDDP, and different models for both the previous and newer scenarios. According to the latter authors, the problem with LARS-WG is that it does not take the newer scenarios. Although, it has been used in studies such as Semenov and Stratonovitch (2015) and Ma et al. (2016) for the newer scenarios, its final version, i.e., LARS-WG6.0, is undergoing some tests. On the other hand, SDSM just involve one GCM, i.e., CanESM2, for the newer scenarios. Therefore, they used the third approach, i.e., NEX-GDDP dataset. The results depicted an enhancement of about 20% of the daily precipitation maxima in the future time period for the region. Chen et al. (2017) investigated the future precipitation extreme events in China by NEX-GDDP dataset and introduced it as a new daily downscaled dataset with high resolution. Moreover, the ability of the dataset in projecting the precipitation extreme events and long-term climate change was assessed, and its power was compared with the CMIP5 GCMs outputs. The conclusions expressed the great competence of the dataset in projecting the spatial patterns of the precipitation extreme events over China. By comparison with the GCMs, NEX-GDDP dataset outputs had a stronger resemblance to the observation data, higher Pearson's correlation, and less relative errors and uncertainty; besides, more details were achieved from local to regional scales. Therefore, they expressed that this dataset, especially for climate change impact's studies in local scales, would probably have more popularity in the future.

In this study, NEX-GDDP downscaled dataset is used to probe climate change in Lali region. Next, in order to predict the impact of climate change on Bibitarkhoun spring for each day, the average of 30 previous days of the climatic variables, i.e., precipitation and temperature, is considered as the inputs of ANN. This approach takes into account the average of the climatic variables of prior days as the network's input so that the spring's lag time response to precipitation is considered. Besides, monthly time step is also considered as the inputs of ANN to simulate the spring's discharge under the climate change for the juxtaposition of the results.

Material and methods

The Lali region is part of Zagros Ranges, located in the northern Khuzestan Province, southwest Iran (Fig. 1). Asmari and Ilam-Sarvak Formations are the main karstic rock units in the studied area. The Bibitarkhoun spring, the largest karstic spring in the region, is located in the southwest part of Pabdeh Anticline. It stems from Asmari Formation and feeds Talug River (Fig. 1). The spring's topographical altitude is about 420 m above sea

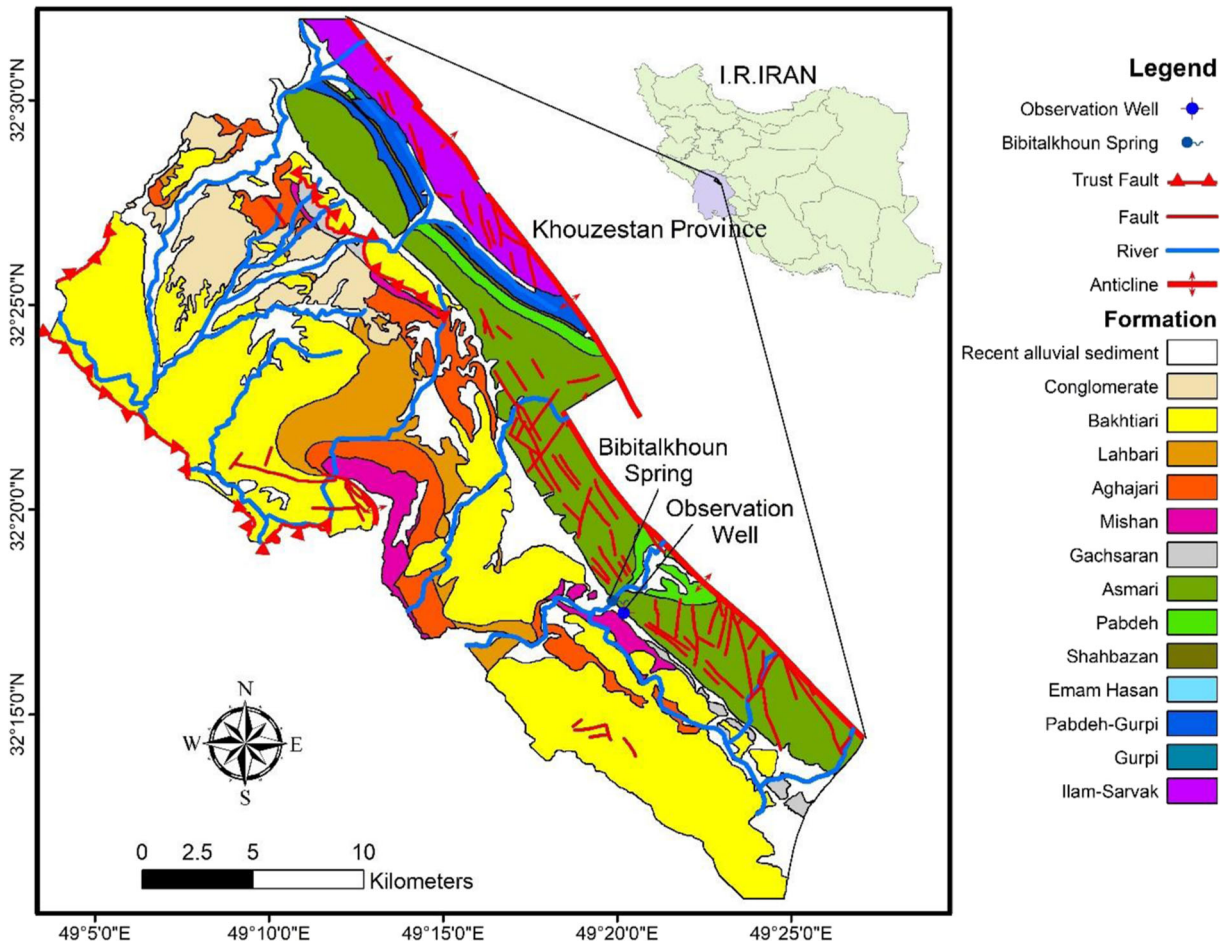

Fig. 1 Lali area and Bibitarkhoun karstic spring and the geological formations of the region

level and the dip of the layers is toward southwest. Groundwater flow in karstic formations is approximately parallel to that of anticline axes, which moves southwestward and finally reaches the river.

Pertinent to the climatic variables, daily observation data is available for time period 2007–2016 (Iran Meteorological Organization 2018), for which the average precipitation and temperature are 396 mm/year and 25.11 °C, respectively. Consequently, according to de Martonne climatic aridity index, climate type is semi-arid.

Climatic variables for the present (1961–1990) and future (2021–2050) time periods under RCP4.5 and RCP8.5 emission scenarios were gathered using NEX-GDDP dataset, which is available online at https://cds.nccs.nasa.gov/nex-gddp/. The time period 2007–2016 was considered as the verification time period to validate the accuracy of this dataset for Lali region. The dataset includes the projection of precipitation, minimum temperature, and maximum temperature for the retrospective period of 1951–2005 and prospective period of 2006–2100, for 21 GCMs under the newer scenarios involving medium low (RCP4.5) and high (RCP8.5) emissions, with the resolution of 0.25°, approximately 25 km (Meinshausen et al. 2011; Taylor et al. 2013; Thrasher and Nemani 2015). Thrasher and Nemani (2015) can be referred for a more nuanced description about the GCMs involved in the dataset. In recent studies about the regional to local climate change, NEX-GDDP dataset has been used (i.e., Ahmadalipour et al. 2017; Bao and Wen 2017; Chen et al. 2017; Donnelly et al. 2016). Introducing corrected bias and high-resolution climate change projections and assessing the climate change impacts on the processes sensitive to climate gradients in local scales by considering the topographical impacts were the main purposes

of producing this dataset (Thrasher et al. 2012). In effect, the topographical impacts influencing the local precipitation events have been considered in the dataset (Bao and Wen 2017).

The Bias-Correction Spatial Disaggregation (BCSD) approach used in NEX-GDDP dataset is an algorithm or a statistical downscaling approach which renders the means and variances of GCMs outputs and the same local observation data (Maurer and Hidalgo 2008; Thrasher et al. 2012; Wood et al. 2002, 2004). The method compares the GCMs outputs and the corresponding observation data; then, the future climatic projections would be adjusted by using the derived information as such that more correlation and real data would be expected. Moreover, the derived spatial data is utilized to insert the GCMs outputs into the grids at higher resolutions. During the downscaling process, the simulated retrospective data, which is used as the training data, is compared with the observation data. Afterwards, the elicited relationships are used to downscale the prospective climatic projections. Global Meteorological Forcing Dataset (GMFD) is used for modeling the surface of the Earth, which is available at Terrestrial Hydrology Research Group, Princeton University, USA (Sheffield et al. 2006). This dataset, which combines the observation and reanalysis data, is available at the spatial resolutions of 0.25°, 0.5°, and 1° and time steps of 3 h, diurnal, and monthly. After the bias-correction stage, the monthly climatic trends are extracted. These trends are preserved in the resultant data and therefore, the probable statistical biases, especially variances, of GCMs outputs are corrected. Then, at the spatial disaggregation stage, the corrected data is inserted into the GMFD data grid. The downscaling method used in NEX-GDDP dataset assumes the relative spatial patterns of precipitation and temperature during the retrospective period are preserved in the future. Except for the bias-correcting and data producing with higher spatial resolution, nothing is added to the original CMIP5 scenarios so that the frequency of precipitation or temperature anomalies is maintained. In this study, for the climatic variables, the average of all GCMs involved in NEX-GDDP dataset is used.

Daily discharge data for Bibitarkhoun spring is available from 21 March 2005 to 31 Decmeber 2016, with some time periods of data gap. The minimum and maximum discharges are approximately 1 and 5 m^3/s, so that maximum per minimum discharge is 5 (KWPA 2005). The spring's catchment area is about 144 km^2 and its dynamic storage is noticeable. The spring's loss curve has unveiled two major discharging regimes. One is conduit with time lag of about 1 month which discharges large volume of water and the other one is a diffuse regime with time lag of about 4–5 months (KWPA 2005). According to the geological log of the observation well in the vicinity of Bibitarkhoun spring (Fig. 1), the karstic Asmari Formation near the spring is not of pure limestone but limestone with layers of marl so the bedrock, which is at the depth of 200 m, is marl.

The ANN toolbox of Matlab R2015a software was used to project the discharge of Bibitarkhoun spring under climate change. The time periods 21 April 2005 to 31 December 2011 and 16 July 2013 to 31 December 2016, with some data gaps as mentioned, have been accounted as the calibration and verification time periods, respectively. ANN has the capability to analyze and simulate non-linear and unknown relationships (Kohzadi et al. 1995). ANN is composed of a set of neurons, which depending on their nexus between different layers, a special architecture is given to the network. A neuron is a simple unit quite similar to a biological neuron. Every neuron receives a signal, processes it, and finally, gives an output (Hagan et al. 2014).

The output of ANN depends on the activation function and for an ANN, the amounts of weights and biases are adjusted by some learning rules so that the input/output relationship reaches a special target. There are different networks which are feedforward, recurrent, and radial basis, with different training algorithms (i.e., Levenberg-Marquardt (LM) and Bayesian regularization (BR)) and various activation functions (i.e., logsig, tansig, and purelin). The interested readers may refer to the related resources such as Hagan et al. (2014) to gain more detailed information regarding the activation functions, learning algorithms, and other facets of networks. The LM training algorithm has been successfully used by different researchers (Anctil et al. 2004; Coulibaly et al. 2000; Coulibaly et al. 2001a, b, c; Maier and Dandy 1998; Maier and Dandy 2000; Toth et al. 2000) and it is more stable and efficient than the other algorithms.

In this study, the feed-forward backpropagation neural network with the LM training algorithm, which is the prototype network in the hydrological studies (Haykin 1999; Friedman and Kandel 1999; Maier and Dandy 2000; Dawson and Wilby 2001; de Vos and Rientjes 2005), was opted.

During the training of the network, the trial and error approach was adopted for selecting the optimum number of hidden layers and neurons by considering some criteria such as the correlation coefficient (R). The calibration (train) dataset was categorized into the training (70%, i.e., 1453 data for the daily approach and 85 data for the monthly approach), validation (15%, i.e., 312 data for the daily approach and 19 data for the monthly approach), and test (15%, i.e., 312 data for the daily approach and 19 data for the monthly approach) groups. By using the validation group, the ANN was prevented from overtraining while the test group demonstrated the capability of ANN to predict the target using inputs not involved during the training process.

While training the network, the observation vis-à-vis the calculation curves of all groups (i.e., training, validation, and test) was being watched to stop training when R was not enhanced considerably.

The statistical criteria used in this study are R, R^2, Nash-Sutcliffe efficiency (NSE), and root mean square error (RMSE), which are defined as the following equations (Gorgij et al. 2017; Jalalkamali et al. 2011; Lu et al. 2018):

$$R = \frac{\left(n\sum_{i=1}^{n} O_i P_i\right) - \left(\sum_{i=1}^{n} O_i \sum_{i=1}^{n} P_i\right)}{\sqrt{\left(n\sum_{i=1}^{n} O_i^2\right) - \left(\sum_{i=1}^{n} O_i\right)^2}\sqrt{\left(n\sum_{i=1}^{n} P_i^2\right) - \left(\sum_{i=1}^{n} P_i\right)^2}}$$

$$R^2 = \left(\frac{\sum_{i=1}^{n}\left(O_i - \overline{O}\right)\left(P_i - \overline{P}\right)}{\sqrt{\left[\sum_{i=1}^{n}\left(O_i - \overline{O}\right)^2\right]\left[\sum_{i=1}^{n}\left(P_i - \overline{P}\right)^2\right]}}\right)^2$$

$$\mathrm{NSE} = 1 - \frac{\sum_{i=1}^{n}\left(O_i - P_i\right)^2}{\sum_{i=1}^{n}\left(O_i - \overline{O}\right)^2}$$

$$\mathrm{RMSE} = \sqrt{\frac{\sum_{i=1}^{N}\left(O_i - P_i\right)^2}{n}}$$

where O_i, P_i, $\bar{O}$, and $\overline{P}$ are the observed, the calculated, the mean of the observed, and the mean of the calculated values, respectively, and n is the number of data. The interval for both R and R^2 is between 0 for the worst condition and 1 for the best condition. The NSE differs from - ∞ to 1, in which 1 is for the best condition. Lower values of RMSE indicate more ability of the model in simulating (Mohanty et al. 2015).

Firstly, all data were normalized using the following equation:

$$X_{\mathrm{norm}} = \frac{X - X_{\mathrm{min}}}{X_{\mathrm{max}} - X_{\mathrm{min}}}$$

In which, X_{norm}, X, X_{min}, and X_{max} are the normalized, actual, minimum, and maximum values, respectively (Chang et al. 2015). The minimum and maximum values of data were considered as such to normalize data between 0.1 and 0.9 instead of 0 and 1; this way, the possible extrapolation of the network is taken into account as well. Masters (1994) demonstrated that the elaborated techniques do not give better results than the linear normalizing methods. The interested reader can refer to different resources, i.e., Masters and Schwartz (1994), Dowla and Rogers (1995), and Swingler (1996), to access enough information about the normalizing approaches.

In this study, despite the statistical criteria, other criteria like the network's output for the verification time period were used to select the optimum network. As already mentioned, given the conduit flow regime with 1-month time lag, for each day, the average of 30 previous days of the climatic variables were considered (approach 1). Moreover, the ANN technique was applied in monthly time step (approach 2) to compare the results and decide whether the network trained with the monthly time step could be confidential or not, especially given the fact that using this time step, there is no conclusive data to apply a verification time period.

Results

Climate change impact on the study area

Although the NEX-GDDP dataset has been already verified, it was verified for Lali region by the observation data for time period 2007–2016. Figure 2 demonstrates the simulation versus observation data for the precipitation, minimum temperature, and maximum temperature for different months of the year. As it is displayed, for precipitation $R^2 = 0.89$ and for minimum and maximum temperatures $R^2 \approx 1$. Hence, the dataset has successfully simulated climatic variables.

Figure 2 also illustrates the precipitation, minimum, and maximum temperatures for different months of the year in the present, and future time periods under RCP4.5 and RCP8.5. There is a decline in the amount of the average precipitation in the future time period and this decline is higher for RCP8.5 as such that for the present, future time period under RCP4.5, and future time period under RCP8.5, the averages of precipitation are 28.66 mm/month (344 mm/year), 27.42 mm/month (329 mm/year), and 27 mm/month (324 mm/year), respectively. Most precipitation occurs during November to April, and precipitation for the present time period is more than that of the future time period under both scenarios during December to March; however, for the other months, it is approximately the same for both time periods or even more for the future time period. Moreover, the minimum and maximum temperatures, with the same trend, would increase in the future time period for all months of the year. The future time period under RCP8.5 demonstrates more enhancement than RCP4.5 so that for the present, future time period under RCP4.5, and future time period under RCP8.5, the minimum

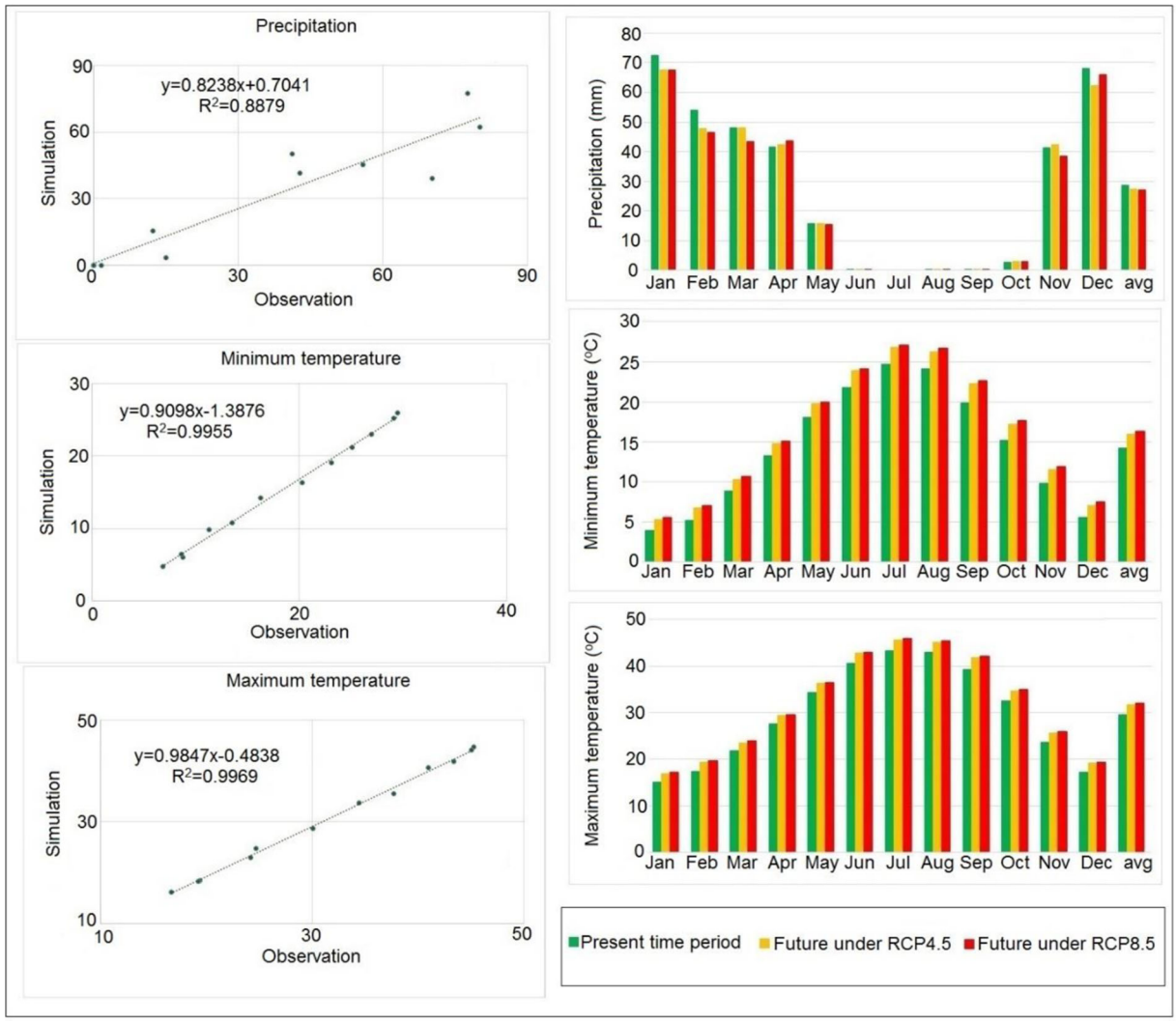

Fig. 2 Climate change results for Lali. On the left: the average of sum monthly GCMs' outputs versus the observation data for the precipitation and the average of mean monthly GCMs' outputs versus the observation data for minimum and maximum temperatures for time period 2007–2016. On the right: outputs of NEX-GDDP dataset for the average of sum monthly precipitation, and the average of mean monthly minimum and maximum temperatures for the present and future time period under RCP4.5 and RCP8.5

temperatures are 14.2, 16, and 16.3 °C, respectively, and the maximum temperatures are 29.6, 31.7, and 31.9 °C, respectively.

The spring's discharge rates simulation

As it was alluded to above, a feed-forward backpropagation neural network with the LM training algorithm was used. One hidden layer with tansig activation function culminated in more realistic outputs. For the output layer, purelin activation function was applied. To determine the number of neurons in the latent layer, the trial and error approach was employed. Additionally, the inputs were selected among the climatic variables namely, precipitation, average temperature, minimum temperature, and maximum temperature, using the trial and error approach. By considering the daily climatic variables as inputs, the ANN is unable to simulate Bibitarkhoun spring's discharge so that for this method the best R is about 0.3. The reason is the time lag in which the precipitation reaches the water table so that the spring's discharge depends on the climatic variables of the previous days or even months, especially for Bibitarkhoun spring, which is the largest spring in the region.

Not only the statistical criteria but also the network's outputs for the verification time period were considered for selecting the suitable network. The other criterion was the visual observation of the network's output for the present and future time periods as it was expected for the spring's discharge values, simulated by ANN, and the precipitation to have a similar trend, as opposite to temperature. Finally, the network was selected by considering all these criteria to decrease the uncertainty of the model so that the results would be more expected in the real world, especially for a karstic system with its complexities.

Therefore, as mentioned before, for every day, the average of 30 previous days was considered as the inputs (approach 1). Figure 3 shows the values of the statistical criteria in relation to the number of neurons for this approach. As Fig. 3 exhibits, by augmenting the number of neurons, the R, R^2, and NSE values would be enhanced and RMSE would be reduced. However, only by considering the statistical criteria, as it is shown in Fig. 3, selecting the exact number of neurons is difficult. Therefore, in combination with the other criteria, a network with precipitation and average temperature as inputs and one hidden layer and 43 neurons gave the best results. Figure 4 demonstrates the simulation versus observation values and also R amounts for different datasets of this network. As it is depicted in Figs. 3 and 4, by considering 43 neurons, R is about 0.63 for different datasets of this network. Further, for this network $R^2 = 0.55$, NSE = 0.55 and RMSE = 0.32 m^3/s so that R^2 and NSE are approximately the maximum and RMSE is approximately the minimum (Fig. 3).

As mentioned before, one of the problems with the karst studies is the paucity of groundwater data, especially because the observation wells are collected monthly. In this condition, there is not enough data to train (calibrate) and also verify the model. Therefore, a good question is whether the test group of the ANN included in the training (calibration) dataset is satisfactorily sufficient to trust the network's results or not. Thus, the average monthly data of Bibitarkhoun spring's discharge (approach 2) was utilized to compare the results with approach 1. In this approach, the best result was yielded for a feed-forward backpropagation network with the LM training algorithm and one hidden layer including 48 neurons and considering precipitation, minimum temperature, and maximum temperature as inputs. Figure 5 displays the network's plot regression for different datasets of the monthly approach, which reveals more R values in relation to approach 1 (Fig. 4), with R values being 0.61, 0.74, and 0.80 for the training, validation, and test datasets, respectively. Moreover, for this network, NSE = 0.52 and RMSE = 0.53 m^3/s.

Figure 6a and b illustrates the network's result for the calibration time period of the karstic spring for approaches 1 and 2, respectively. For approach 2, the network's output does not match the observation data as well as approach 1, especially for year 2012, because of probably the data gap between 2011 and 2012; however, the network has simulated the peak discharges well enough.

As shown in Fig. 6a, for approach 1, the model has been calibrated well and now it must be verified with the data not included during the training of the network. Figure 7a proffers the selected network's result of approach 1 for the verification time period. As it is shown, the network's output demonstrates the same trend as the observation data for the verification time period; however, it slightly underestimates the peak flows and somewhat overestimates the low flows for some part of the curve.

The higher values of the statistical criteria do not always indicate the better capability of the network;

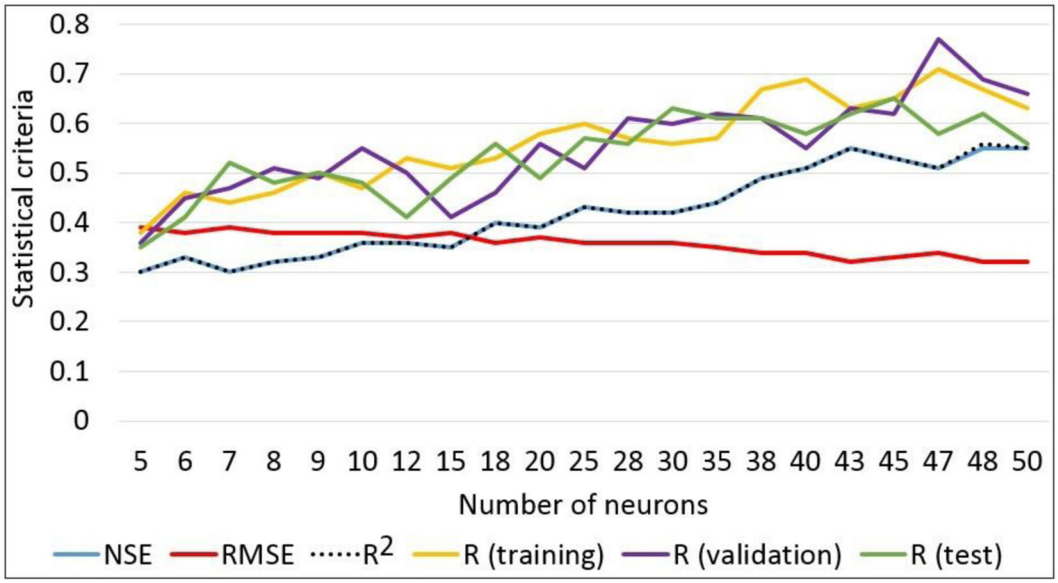

Fig. 3 Values of different statistical criteria versus the number of neurons for different datasets by considering the average of 30 previous days for the climatic variables

Fig. 7a demonstrates the result of a network with 48 neurons for the verification time period, which has more values of the statistical criteria, as it is shown in Fig. 3. Nevertheless, the network's output for the verification time period is worse than that of the network with 43 neurons.

Figure 8a demonstrates the impact of climate change on Bibitarkhoun spring for approach 1. The average discharge of the spring is about 2.25 m^3/s for the observation data. It does not change considerably for the present and future time period under both scenarios and is approximately 2.3 m^3/s. However, the spring's discharge varies during the different months of the year for the present and future time periods. For instance, for November to March (cold/wet period), it is higher for the present time period and for the other months (warm/dry period), it is higher for the future time period. The point is for the future time period under RCP4.5 and RCP8.5, the spring's discharge does not differ significantly. The discharges of the present and observation time periods have a fairly akin trend and some perceived dissimilarities could boil down to (1) the different time periods of the observation and present time periods and (2) the data for the present time period has been simulated by the ANN and includes some uncertainties. However, the condition is somewhat different for the future time period under both scenarios, especially for the warm/dry months, and this is the impact of the climate change on Bibitarkhoun karstic spring.

Finally, Fig. 8b demonstrates the impact of climate change on Bibitarkhoun spring for approach 2. Like approach 1 (Fig. 8a), the spring's discharge does not later substantially for the present and future time periods in both scenarios; the average discharge is about 2.7 m^3/s for the present and 2.65 m^3/s for the future time periods under both scenarios. As it was noticed before, for the observation data, the average spring's discharge is about 2.25 m^3/s and for approach 1, the average spring's discharge was 2.3 for the present and future time periods under both scenarios, which is remarkably close to the observation data. Although for approach 1, the spring's discharge is higher for the cold/wet period during the present time period than that of the future time period and for the warm/dry period the situation is vice versa, this pattern is not regularly observed in approach 2. Moreover, for approach 1, the spring's discharge differs slightly for the months of the year although it changes more obviously for approach 2. Bibitarkhoun is the largest spring in the region with a large catchment area and its observation data changes slightly during the year (as shown in Fig. 8a and b; hence, the results of the approach 1 are more expectable.

In sum, it can be construed that the statistical criteria exclusively do not indicate better capabilities of the network to simulate the spring's discharge under climate change and it is important to have a different dataset as the verification time period.

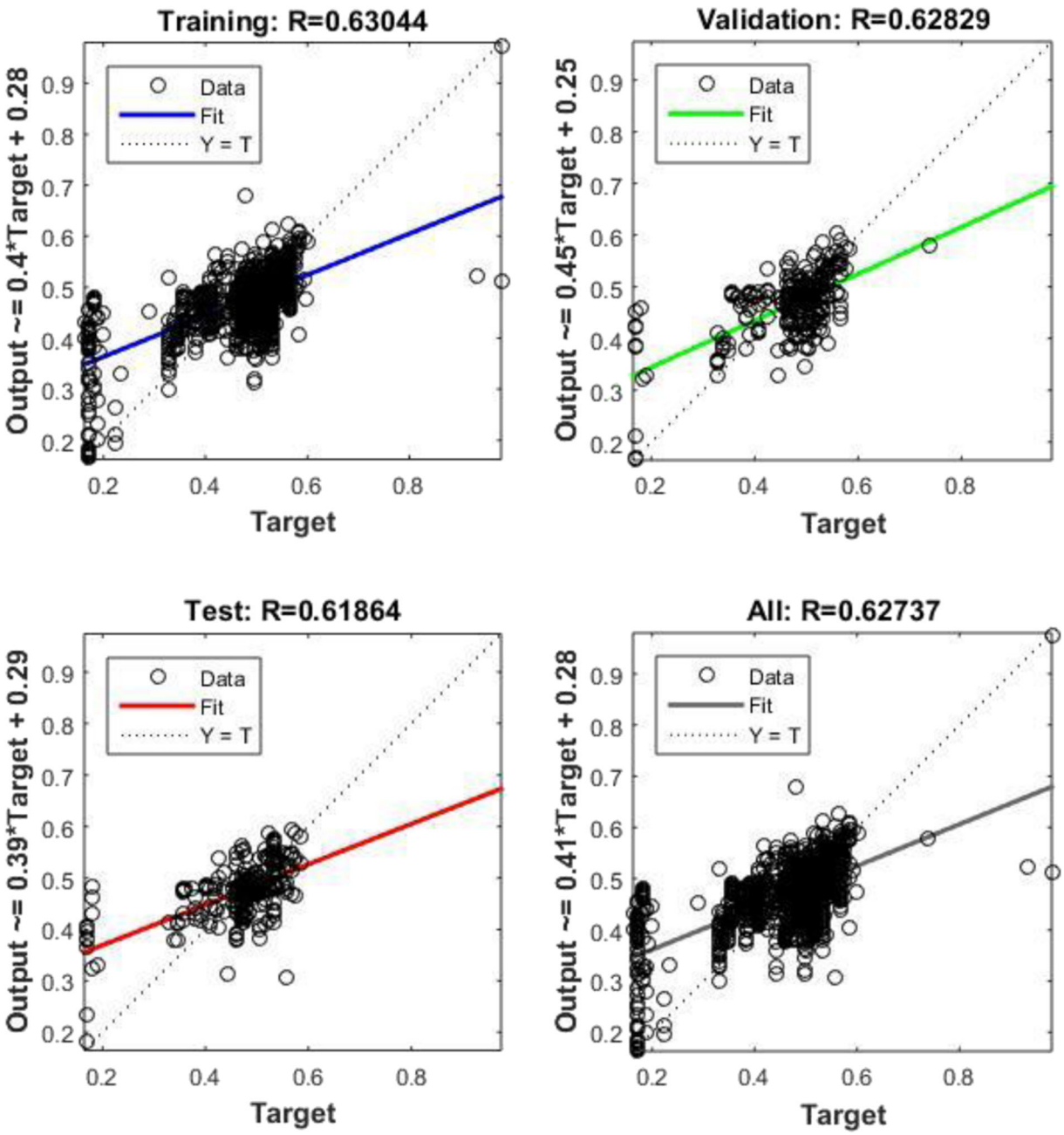

Fig. 4 Target (observation) against output (simulation) data for the daily time step by considering the average of 30 previous days for the climatic variables for training, validation, test and all datasets. As it is shown, values are normalized

Discussion

Climate change

The downscaling method used in NEX-GDDP dataset is a statistical approach considering two emission scenarios, i.e., RCP4.5 and RCP8.5. A multi-model ensemble includes many models produced by different research modeling centers in the world. However, the models' simulations almost correlate because of similarity in dynamical cores and physical parameterizations; moreover, same observation data have been included in them. Therefore, they constitute a cluster in relation to

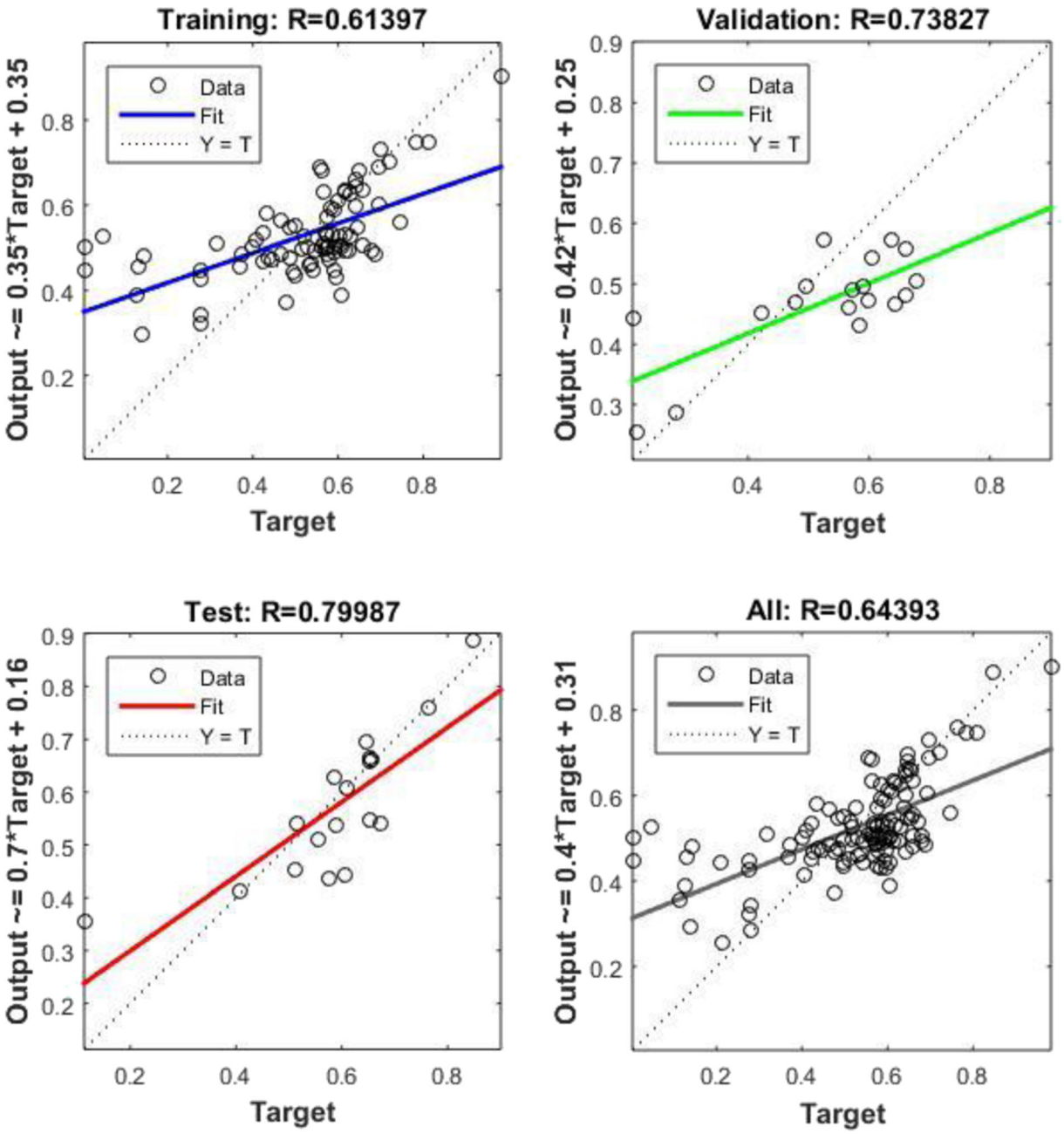

Fig. 5 Target (observation) data against output (simulation) data by considering monthly time step for training, validation, test and all datasets. As it is shown, values are normalized

their simulation of climate change (Knutti et al. 2013; Masson and Knutti 2011).

NEX-GDDP dataset project the minimum and maximum temperatures with $R^2 \approx 1$ and precipitation with $R^2 = 0.89$. These results are corroborated by Raghavan et al. (2018). They assessed the performance of NEX-GDDP data over Southeast Asia and concluded this dataset demonstrates more uncertainties in the projection of precipitation than temperature.

Precipitation is an important factor of the global water cycle and due to its interactions with different parts of climate demonstrates complex features (Jia et al. 2011). The incidence of precipitation requires numerous circumstances to occur in relation to many

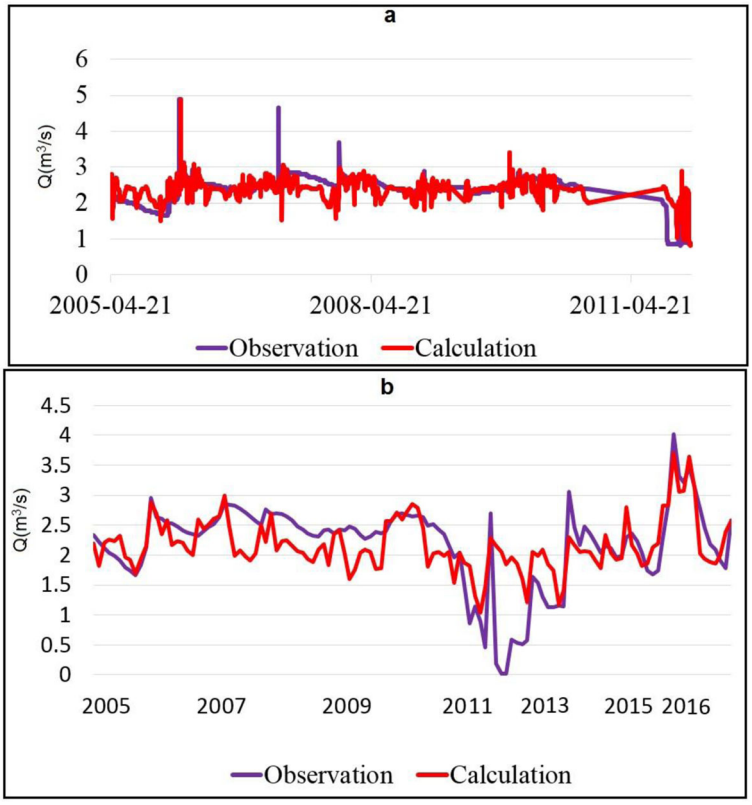

Fig. 6 The calibration results for the selected network, one hidden layer with 43 neurons, for daily time step by considering the average of 30 previous days for the climatic variables (a) and the calibration results for the selected network, one hidden layer with 48 neurons, for monthly time step (b)

factors, e.g., humidity and coldness (Mohammadi and Masoudian 2010).

The projection of precipitation is more challenging than temperature in Lali region. The atmospheric instabilities and precipitation occurrences in southwest Iran, including Lali region, are generally influenced by Sudanese systems which result in heavy precipitations (Mohammadi et al. 2013). The convective motions in combination with the western and southern winds cause thunderstorms in southwest Iran (Ataei et al. 2016). Indeed, arid and semi-arid regions face heavy rainfalls with great spatial and temporal variabilities. Moreover, the scarcity of precipitation synoptic stations prevents the accurate estimation of precipitation and its spatial distribution.

The karstic aquifer simulation

This is a local case study in which climate has been related to the hydrologic model to simulate Asmari karstic aquifer. However, regional and global studies can simulate the overall recharge trend of the aquifer in the future time period by combining the low-resolution climate models with the hydrologic models (Taylor et al. 2013). In this context, NEX-GDDP dataset cannot be employed since they have been already downscaled.

The model's structure may influence the outcomes of groundwater simulation (Moeck et al. 2016). Even though ANN has been utilized in this study, many modeling and machine learning approaches exist that can relate the climate change with groundwater. In relation to groundwater forecasting, Djurovic et al. (2015) assessed ANN and adaptive neurofuzzy inference system (ANFIS), Mohanty et al. (2015) utilized ANN by adopting gradient decent with momentum and adaptive learning rate backpropagation (GDX) algorithm, Nourani et al. (2015) employed ANN after treating the wavelet-entropy data, Yoon et al. (2016) applied both ANN and support vector machine (SVM), Choubin and Malekian (2017) integrated ANN and autoregressive integrated moving average (ARIMA), Gorgij et al. (2017) used ANN and genetic programming, and Sahoo et al. (2017) used spectral analysis, machine learning, and uncertainty analysis by adopting mutual information, genetic algorithms, and

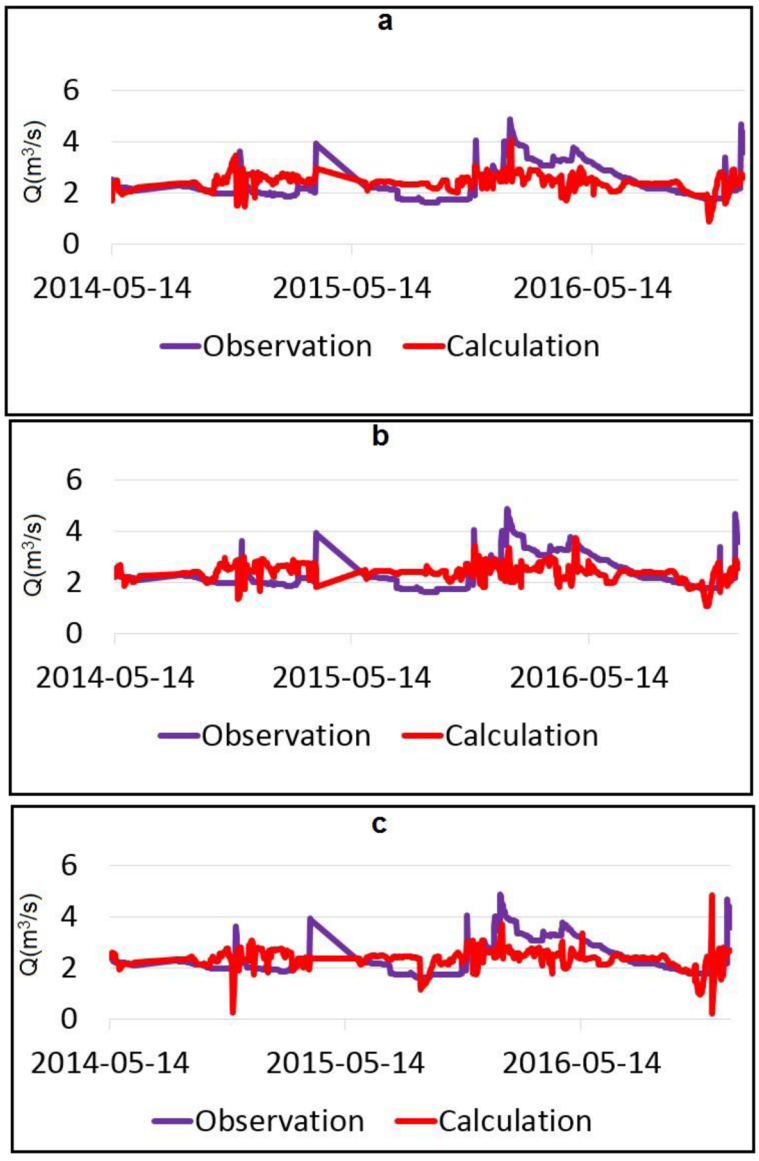

Fig. 7 The verification results for the selected network, one hidden layer with 43 neurons (a), a network with one hidden layer and 48 neurons (b), and a network with 2 hidden layers with 28 neurons in the first hidden layer and 18 neurons for the second hidden layer (c) all for the daily time step by considering the average of 30 previous days for the climatic variables

lag analysis for the input data selection. Anyway, various aspects of the hydrologic model selection have not been represented in this study.

Applying intricate models is not always preferable than simple models. The physical models may not demonstrate any advantages over the simple models; they may even include calculation problems (Jakeman and Hornberger 1993; Refsgaard 1996). Indeed, the ANNs with one hidden layer containing finite number of neurons can estimate continuous functions; this is called the universal approximation theorem (Nielsen 1987).

The main problem of the ANN is that it does not have the physical concepts and selecting the network architecture and other training factors is experimental (Hu et al. 2008). Nevertheless, in relation to the physical-based models, it is usually less time consuming (Smiatek et al. 2013). The condition may be even worse if different networks and training algorithms are considered too. However, the feed-forward backpropagation with the LM training algorithm usually gives the best results in hydrology. Trichakis et al. (2011) stated that there are some parameters like hydraulic conductivity which are constant and variables like precipitation which differ over time. The variables are the inputs of the ANN and the problem with the parameters is solved by the weights. In fact, a benefit of the ANN is that it

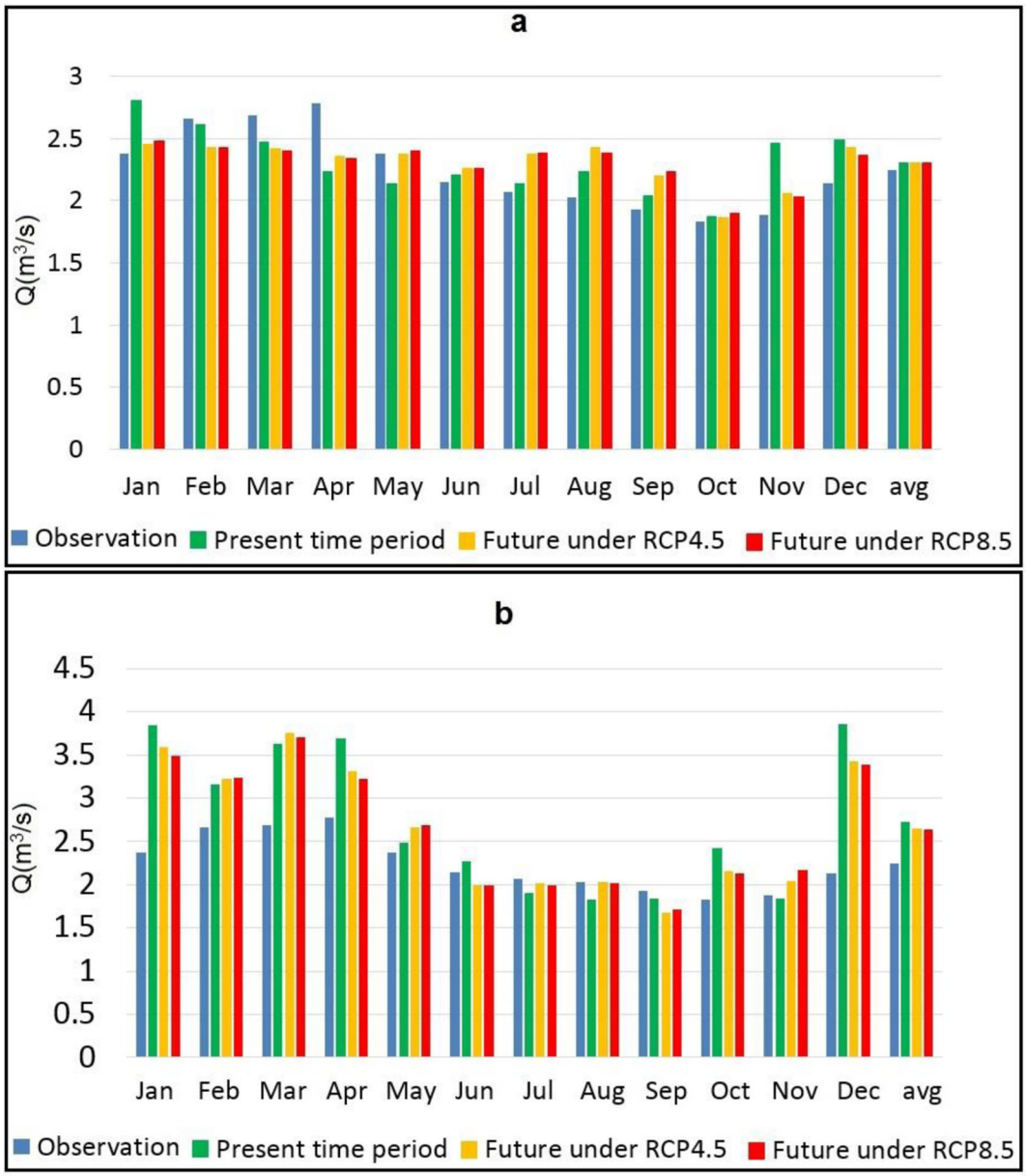

Fig. 8 The discharge of Bibitarkhoun spring for the observation (2005–2016), present time period (1961–1990) and future time period (2021–2050) under RCP4.5 and RCP8.5 by considering the average of 30 previous days for the climatic variables (a) and monthly time step (b)

solely takes the climatological variables as inputs and hydrological parameters are considered as the network's weights when trained.

As Chester (1990) stated, the network with 2 hidden layers usually gives better results for prediction, because the local and global features of the fitting function would be recognized by the first and second hidden layers, respectively. Table 1 shows the best results for the simulation of the discharge of Bibitarkhoun spring for approach 1 (considering the average of 30 previous days for the climatic variables) by considering 2 hidden layers. Based upon Table 1, the best R (i.e., 0.71 for the training, 0.77 for the validation, and 0.73 for the test dataset), R^2 (i.e., 0.5), NSE (i.e., 0.5), and RMSE (i.e., 0.31) values are germane to the architecture with 28 neurons in the first hidden layer and 18 neurons in the

Table 1 The best values of different statistical criteria for networks with 2 hidden layers for the daily time step by considering the average of 30 previous days for the climatic variables

Array	Number of neurons		NSE	RMSE	R^2	R			
	Layer 1	Layer 2				Training	Validation	Test	All
1	26	15	0.44	0.32	0.44	0.68	0.69	0.66	0.68
2	26	18	0.45	0.67	0.45	0.57	0.69	0.63	0.60
3	28	15	0.46	0.32	0.45	0.68	0.66	0.62	0.67
4	28	18	0.50	0.31	0.50	0.71	0.77	0.73	0.72

second hidden layer. Figure 7c demonstrates this network's output for the verification time period, which is in relation to the network with one hidden layer (Fig. 7a), and reveals some deviations as such that the prediction of this network could not be entirely reliable. Indeed, complex architecture of ANN does not always give the best results, because the increase in the inputs and hidden layers would accumulate errors (Hu et al. 2008).

Even though the ANN gave the best results by considering the average of 30 previous days of the climatic variables (approach 1), the time lag between precipitation and the spring's discharge rates was evaluated to see whether this time period has physical meaning or not. Thence, the R and NSE values were calculated by considering various time lags between precipitation and the spring's discharge rates (Fig. 9). The R value becomes the maximum for the time lag of 30 days; further, the NSE values reach a maximum and stable situation after the time lag of 30 days (Fig. 9). Therefore, the time lag between precipitation and the spring's discharge rates is approximately 30 days.

Trichakis et al. (2011) for an ANN simulation divided data into two groups: 80% for the training and 20% for test. They stated that using the test data not included during the training stage can examine the ability of the network to generalize, expand, interpolate, or extrapolate. Therefore, as for Bibitarkhoun spring simulation, it is of the essence to scrutinize the network's ability for generalization alongside the statistical criteria like R.

The climate data is mainly considered as the input of ANN (Coppola et al. 2005; Djurovic et al. 2015; Ghose et al. 2010; Lallahem et al. 2005; Tsanis et al. 2008); however, this is not always correct such that Uddameri

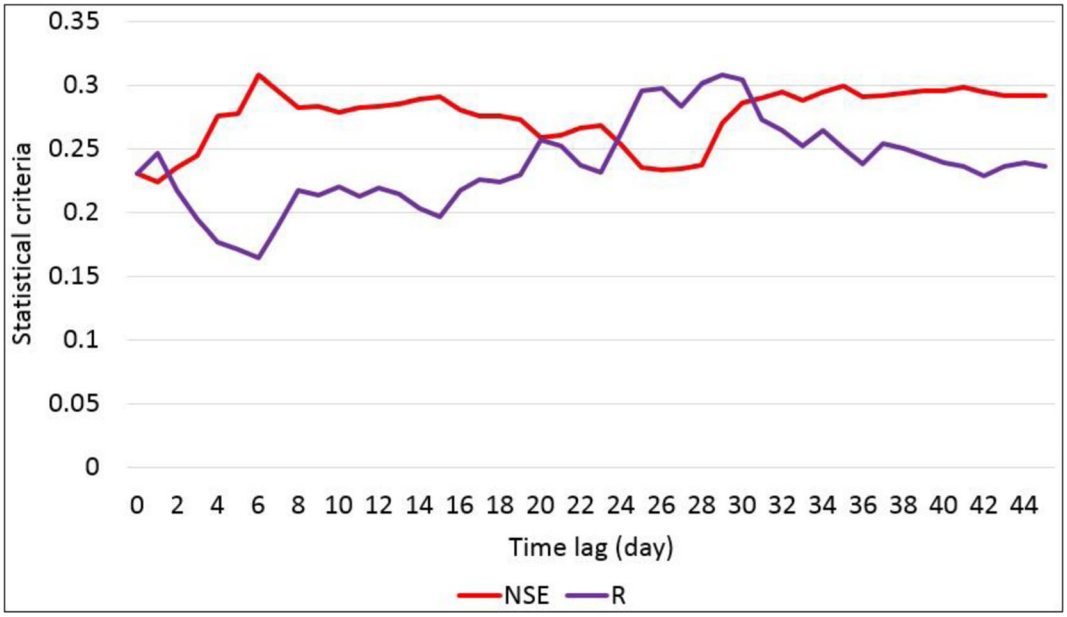

Fig. 9 The statistical criteria for different time lags between precipitation and discharge of Bibitarkhoun spring

(2007) could not find a relationship between the climatic variables and groundwater level.

The proper combination of the climatic variables, which lead to a better result, must be selected. In this study, the following combinations were deemed:

a) Precipitation
b) Precipitation and average temperature
c) Precipitation, minimum temperature, and maximum temperature
d) Precipitation, minimum temperature, maximum temperature, and average temperature

Combinations b and c introduced the best results for approach 1 and approach 2, respectively.

In relation to the network's simulation for the calibration and verification time periods (Fig. 6a and Fig. 7a), it can be stated that there are some data gaps in the observation data and more coincidence may have been resulted if such condition did not exist.

With regard to choosing the calibration and verification time periods, it is safe to add that the shorter the calibration time period, the more unstable the model (Hu et al. 2008). Therefore, a longer time period was selected for the calibration (2005–2011). In fact, as Hu et al. (2008) emphasized, changing the calibration and verification time periods and comparing the statistical criteria can be considered as another way to select the best network. For Bibitarkhoun spring, considering the calibration time period 2005–2011 represented better results.

For a karstic spring, the ratio Q_{max}/Q_{min} is 1.24–5.89 for semi-arid regions and 10–1000 for the humid regions (He et al. 1997). By considering this ratio, it is crystal clear that the response of the karstic aquifers to the climatic variables is longer for the semi-arid regions and therefore, its simulation is more arduous than that of the humid regions. In effect, different storages in karst of the semi-arid regions provide a vast reservoir for the precipitation and a large basin even more than thousands of square kilometers may exist for a karstic spring (Han et al. 1993; Ma et al. 2004). In the case of Bibitarkhoun spring, which is located in a semi-arid region, these also influence the results and therefore, that is a great advantage of ANN to simulate karst in such difficult circumstances with scarce data.

Finally, various factors such as transmissivity and pumping wells can change the sensibility of the geologic formations to climate change (Nassery et al. 2016). Further, the sensibility of aquifers to climate change can differ depending on different recharge mechanisms (Flint and Flint 2014).

Conclusions

NEX-GDDP data successfully simulated the climatic variables in the Lali region such that for precipitation $R^2 = 0.89$, and for minimum and maximum temperatures $R^2 \approx 1$. Not only does NEX-GDDP dataset perform better for temperature than precipitation (Raghavan et al. 2018) but it is also the climatic characteristics of the Lali region that makes it difficult to simulate precipitation.

There exists no pumping well in the vicinity of Bibtarkhoun spring; therefore, the climate change impact on this spring can be studied without an uncertainty of pumping wells which is an important source of uncertainty. That said, for the first time, a non-numerical hydrological model viz. ANN was postulated to simulate the impact of climate change on Bibitarkhoun karstic spring under RCP4.5 and RCP8.5 emission scenarios with the use of the climatic variables as inputs.

Bibitarkhoun spring's discharge was modeled using the average of 30 previous days for the climatic variables (approach 1). For a feed-forward backpropagation network with LM training algorithm, the best results were achieved for one hidden layer and 43 neurons with the precipitation and average temperature as inputs. For this network, $R = 0.63$, $R^2 = 0.55$, NSE = 0.55, and RMSE = 0.32 m^3/s, and even though larger values of the statistical criteria could be also achieved—for example, for a network with 2 hidden layers including 28 and 18 neurons for the first and second hidden layers, respectively—the simulated data for the verification time period did not demonstrate satisfactory results. The average discharge of the spring, which is 2.3 m^3/s, does not change considerably for the present and future time periods under either of the scenarios. However, the spring's discharge varies during the different months of the year for the present and future time periods; for November to March, it is higher for the present time period and for the other months, it is higher for the future time period. Regarding the emission scenarios, the spring's discharge does not change substantially.

Moreover, the impact of the climate change on Bibitarkhoun spring was determined for the monthly time step (approach 2). In this approach, the average

spring's discharge does not also considerably change for the present and future time periods under both of the scenarios; it is roughly 2.7 m^3/s for the present time period and 2.65 m^3/s for the future time period in both scenarios. It shall not go amiss to mention that the spring's discharge changes more obviously for the months of the year. However, in this approach, due to data scarcity, the verification time period does not exist and it is not as trustworthy as approach 1.

Finally, the results of this study for a region with no pumping wells and human influences demonstrate no significant variations in the karstic spring's discharge rates by considering either of the approaches. Therefore, the impact of climate change on groundwater resources should be studied more precisely, especially for the pristine lands like the Lali region.

Acknowledgments The authors would like to thank Khouzestan Water and Power Authority for providing Bibitarkhoun spring data. We thank the editor and three anonymous reviewers for their constructive comments on the earlier manuscript, which lead to the improvement of the article.

References

Adiat, K. A. N., Ajayi, O. F., Akinlalu, A. A., & Tijani, I. B. (2020). Prediction of groundwater level in basement complex terrain using artificial neural network: a case of Ijebu-Jesa, southwestern Nigeria. *Applied Water Science, 10*, 8. https://doi.org/10.1007/s13201-019-1094-6.

Ahmadalipour, A., Moradkhani, H., & Svoboda, M. (2017). Centennial drought outlook over the CONUS using NASA-NEX downscaled climate ensemble. *International Journal of Climatology, 37*(5), 2477–2491.

Anctil, F., Perrin, C., & Andréassian, V. (2004). Impact of the length of observed records on the performance of ANN and of conceptual parsimonious rainfall-runoff forecasting models. *Environmental Modelling and Software, 19*(4), 357–368.

Ataei, H., Pouladi, R., & Fanaei, R. (2016). The statistical-synoptic evaluation of heavy precipitation events in Khouzestan Province. 1st international conference on natural hazards and environmental crises in Iran, strategies and challenges, Ardabil, Iran, 1-16 [in Persian].

Bao, Y., & Wen, X. (2017). Projection of China's near-and long-term climate in a new high-resolution daily downscaled dataset NEX-GDDP. *Journal of Meteorological Research, 31*(1), 236–249.

Bardossy, A. (2007). Calibration of hydrological model parameters for ungauged catchments. *Hydrology and Earth System Sciences, 11*(2), 703–710.

Brenner, S., Coxon, G., Howden, N. J. K., Freer, J., & Hartmann, A. (2018). Process-based modelling to evaluate simulated groundwater levels and frequencies in a chalk catchment in South-Western England. *Natural Hazards and Earth System Sciences, 18*, 445–461.

Chang, J., Wang, G., & Mao, T. (2015). Simulation and prediction of supra-permafrost groundwater level variation in response to climate change using a neural network model. *Journal of Hydrology, 529*, 1211–1220.

Chen, H. P., Sun, J. Q., & Li, H. X. (2017). Future changes in precipitation extremes over China using the NEX-GDDP high-resolution daily downscaled data-set. *Atmospheric and Oceanic Science Letters, 10*(6), 403–410.

Chester, D. L. (1990). Why two hidden layers are better than one. Paper presented at the Proc. IJCNN, Washington, DC, 1, 265–268.

Choubin, B., & Malekian, A. (2017). Combined gamma and M-test-based ANN and ARIMA models for groundwater fluctuation forecasting in semiarid regions. *Environmental Earth Sciences, 2017*(76), 538. https://doi.org/10.1007/s12665-017-6870-8.

Coppola, E. A., Rana, A. J., Poulton, M. M., Szidarovszky, F., & Uhl, V. W. (2005). A neural network model for predicting aquifer water level elevations. *Ground Water, 43*(2), 231–241.

Coulibaly, P., Anctil, F., & Bobee, B. (2000). Daily reservoir inflow forecasting using artificial neural networks with stopped training approach. *Journal of Hydrology, 230*(3–4), 244–257.

Coulibaly, P., Anctil, F., Aravena, R., & Bobée, B. (2001a). Artificial neural network modeling of water table depth fluctuations. *Water Resources Research, 37*(4), 885–896.

Coulibaly, P., Anctil, F., & Bobee, B. (2001b). Multivariate reservoir inflow forecasting using temporal neural networks. *Journal of Hydrologic Engineering, 6*(5), 367–376.

Coulibaly, P., Bobée, B., & Anctil, F. (2001c). Improving extreme hydrologic events forecasting using a new criterion for artificial neural network selection. *Hydrological Processes, 15*(8), 1533–1536.

Daksiya, V., Mandapaka, P. V., & Lo, E. Y. M. (2017). A comparative frequency analysis of maximum daily rainfall for a SE Asian region under current and future climate conditions. *Advances in Meteorology, 2017*(2), 1–16.

Daliakopoulos, I. N., Coulibaly, P., & Tsanis, I. K. (2005). Groundwater level forecasting using artificial neural networks. *Journal of Hydrology, 309*(1–4), 229–240.

Dawson, C. W., & Wilby, R. L. (2001). Hydrological modelling using artificial neural networks. *Progress in Physical Geography: Earth and Environment, 25*(1), 80–108.

De Vos, N. J., & Rientjes, T. H. M. (2005). Constraints of artificial neural networks for rainfall-runoff modelling: trade-offs in hydrological state representation and model evaluation. *Hydrology and Earth System Sciences, 2*(1), 365–415.

Djurovic, N., Domazet, M., Stricevic, R., Pocuca, V., Spalevic, V., Pivic, R., Gregoric, E., & Domazet, U. (2015). Comparison of groundwater level models based on artificial neural networks and ANFIS. *The Scientific World Journal, 2015*, 1–13. https://doi.org/10.1155/2015/742138.

Donnelly, M. A. P., Marcantonio, M., Melton, F. S., & Barker, C. M. (2016). Mapping past, present, and future climatic suitability for invasive Aedes aegypti and *Aedes albopictus* in the United States: a process-based modeling approach using

CMIP5 downscaled climate scenarios. Paper presented at the AGU Fall Meeting Abstracts.

Dowla, F. U., & Rogers, L. L. (1995). *Solving problems in environmental engineering and geosciences with artificial neural networks*. MIT Press 239p.

Drew, D., & Hötzl, H. (1999). *Karst hydrogeology and human activities: impacts, consequences and implications* (1st ed.). Routledge Publishing 340p.

Flint, L. E., & Flint, A. L. (2014). California basin characterization model: a dataset of historical and future hydrologic response to climate change, U.S. *Geological Survey Data Release*. https://doi.org/10.5066/F76T0JPB.

Ford, D. C., & Williams, P. W. (1989). Karst hydrogeology and geomorphology. John Wiley Publishing, Chichester, 576p.

Friedman, M., & Kandel, A. (1999). *Introduction to pattern recognition: statistical, structural, neural and fuzzy logic approaches* (Vol. 32). World Scientific Publishing Company 344p.

Ghose, D. K., Panda, S. S., & Swain, P. C. (2010). Prediction of water table depth in western region, Orissa using BPNN and RBFN neural networks. *Journal of Hydrology, 394*(3–4), 296–304.

Goldscheider, N., & Drew, D. (2014). Methods in karst hydrogeology: IAH: International contributions to hydrogeology, 26. CRC Press, 280p.

Gorgij, A. D., Kisi, O., & Moghadam, A. A. (2017). Groundwater budget forecasting, using hybrid wavelet-ANN-GP modelling: a case study of Azarshahr Plain, East Azerbaijan, Iran. *Hydrology Research, 48*(2), 455–467.

Hagan, M. T., Demuth, H. B., Beale, M. H., & Jessus, O. D. (2014). *Neural network design* (2nd ed.). Martin Hagan 800p.

Han, X., Lu, R., & Li, Q. (1993). *Karst water system—case study of big karst springs in Shanxi Province*. Beijing: Geology Press.

Haykin, S. (1999). *Neural networks, a comprehensive foundation* (2nd ed.). Prentice-hall publishing 768p.

He, Y., Han, B., & Xue, C. (1997). Study of karstic-water in China. Tongji University Press: Shanghai (in Chinese with English abstract). https://cds.nccs.nasa.gov/nex-gddp/.

Hu, C., Hao, Y., Yeh, T. C. J., Pang, B., & Wu, Z. (2008). Simulation of spring flows from a karst aquifer with an artificial neural network. *Hydrological Processes, 22*(5), 596–604.

IPCC. (2013). Climate change 2013: the physical science basis: contribution of working group I to the fifth assessment report of the intergovernmental panel on climate change. Cambridge University Press.

Iran Meteorological Organization. (2018). Climate data including daily precipitation, temperature and solar radiation from 2007–2016 for Lali synoptic station in Excel Format.

Jakeman, A. J., & Hornberger, G. M. (1993). How much complexity is warranted in a rainfall runoff model? *Water Resources Research, 29*, 2637–2649.

Jalalkamali, A., Sedghi, H., & Mansouri, M. (2011). Monthly groundwater level prediction using ANN and neuro-fuzzy models: a case study on Kerman plain, Iran. *Journal of Hydroinformatics, 13*(4), 867–876.

Jia, S., Zhu, W., Lu, A., & Yan, T. (2011). A statistical spatial downscaling algorithm of TRMM precipitation based on NDVI and DEM in the Qaidam Basin of China. *Remote Sensing of Environment, 115*, 3069–3079.

Khouzestan Water and Power Authority. (2005). Semi-analytical report of hydrogeology of Lali.

Knutti, R., Masson, D., & Gettelman, A. (2013). Climate model genealogy: generation CMIP5 and how we got there. *Geophysical Research Letters, 40*(6), 1194–1199.

Kohzadi, N., Boyd, M. S., Kaastra, I., Kermanshahi, B. S., & Scuse, D. (1995). Neural networks for forecasting: an introduction. *Canadian Journal of Agricultural Economics, 43*(3), 463–474.

Lallahem, S., Mania, J., Hani, A., & Najjar, Y. (2005). On the use of neural networks to evaluate groundwater levels in fractured media. *Journal of Hydrology, 307*(1–4), 92–111.

Lu, J., Jia, L., Menenti, M., Yan, Y., Zheng, C., & Zhou, J. (2018). Performance of the standardized precipitation index based on the TMPA and CMORPH precipitation products for drought monitoring in China. *IEEE Journal of Selected Topics in Applied Earth Observations and Remote Sensing, 11*, 1387–1396. https://doi.org/10.1109/JSTARS.2018.2810163.

Ma, T., Wang, Y., & Guo, Q. (2004). Response of carbonate aquifer to climate change in northern China: a case study at the Shentou karst springs. *Journal of Hydrology, 297*(1–4), 274–284.

Ma, C., Pan, S., Wang, G., Liao, Y., & Xu, Y. P. (2016). Changes in precipitation and temperature in Xiangjiang River Basin, China. *Theoretical Applied Climatology, 123*, 859–871.

Maier, H. R., & Dandy, G. C. (1998). Understanding the behaviour and optimising the performance of back-propagation neural networks: an empirical study. *Environmental Modelling and Software, 13*(2), 179–191.

Maier, H. R., Dandy, G. C. (2000). Neural networks for the prediction and forecasting of water resources variables: a review of modelling issues and applications. Environmental Modelling and Software, 15(1), 101–124.

Masson, D., & Knutti, R. (2011). Spatial-scale dependence of climate model performance in the CMIP3 ensemble. *Journal of Climate, 24*(11), 2680–2692.

Masters, T., & Schwartz, M. (1994). Practical neural network recipes in C++. *IEEE Transactions on Neural Networks, 5*(5), 853–853.

Maurer, E. P., & Hidalgo, H. G. (2007). Utility of daily vs. monthly large-scale climate data: an intercomparison of two statistical downscaling methods. *Hydrology and Earth System Sciences Discussions, 4*,(5), 3413–3440.

Meinshausen, M., Smith, S. J., Calvin, K., Daniel, J. S., Kainuma, M. L. T., Lamarque, J. F. , Matsumoto, K., Montzka, S. A., Raper, S. C. B., Riahi, K., Thomson, A., Velders, G. J. M., & van Vuuren, D. P. P. (2011). The RCP greenhouse gas concentrations and their extensions from 1765 to 2300. *Climatic Change,* 109(1–2), 213–241.

Milanovic, P. T. (1981). *Karst hydrogeology* (434p). Water Resources Publications.

Moeck, C., Brunner, P., & Hunkeler, D. (2016). The influence of model structure on groundwater recharge rates in climate-change impact studies. *Hydrogeology Journal, 24*(5), 1171–1184.

Mohammadi, B., & Masoudian, S. A. (2010). Synoptic analysis of heavy precipitation events in Iran. *Geography and Development, 8*(19), 47–70 [in Persian].

Mohammadi, H., Fatahi, A., Shamsipour, A. A., & Akbari, M. (2013). The dynamical analysis of Sudanese air masses and heavy precipitation events in Southwest Iran. *Applied Investigations of Geographic Sciences, 12*(24), 7–24 [in Persian].

Mohanty, S., Jha, M. K., Raul, S. K., Panda, R. K., & Sudheer, K. P. (2015). Using artificial neural network approach for simultaneous forecasting of weekly groundwater levels at multiple sites. *Water Resources Management, 29*, 5521–5532.

Morrissey, P., Gill, L., Naughton, O., McCromack, T., & Johnston, P. (2018). Groundwater flood modelling in the karst lowlands of South Galway. *Irish National Hydrology Conference, 2018*, 100–115.

Nassery, H. (1992). Hydrogeology study of karstic springs in Doroudzan dam basin. (master thesis), Shiraz University, Iran.

Nassery, H. R., Salami, H., & Bavani, A. M. (2016). Adaptation strategies in alluvial aquifer under future climate change (case study: Hamadan aquifer, west of Iran). 7th international Water resources management conference of ICWRS, Bochum, Germany.

Nielsen, R. H. (1987). Counterpropagation networks. *Applied Optics, 26*(23), 4979–4984.

Nourani, V., Alami, M. T., & Vousoughi, F. D. (2015). Wavelet-entropy data pre-processing approach for ANN-based groundwater level modeling. *Journal of Hydrology, 524*, 255–269.

Pla, C., Valdes-Abellan, J., Tenza-Abril, A. J., & Benavente, D. (2016). Predicting daily water table fluctuations in karstic aquifers from GIS-based modelling, climatic settings and extraction wells. *Water Resources Management, 30*(7), 2531–2545.

Pollacco, J. A. P., Ugalde, J. M. S., Angulo-Jaramillo, R., Braud, I., & Saugier, B. (2008). A linking test to reduce the number of hydraulic parameters necessary to simulate groundwater recharge in unsaturated zone. *Advances in Water Resources, 31*(2), 355–369.

Raghavan, S. V., Hur, J., & Liong, S. (2018). Evaluations of NASA NEX-GDDP data over Southeast Asia: present and future climates. *Climatic Change, 148*, 503–518.

Refsgaard, J. C. (1996). Model and data requirements for simulation of runoff and land surface processes in relation to global circulation models. Global environmental change and land surface processes in hydrology: the trial and tribulations of modelling and measuring. In: Sorooshian, S., Gupta, H., & Rodda, J. (Eds.), NATO ASI, Springer-Verlag, New York, 1(46), 423–445.

Sahoo, S., Russo, T. A., Elliott, J., & Foster, I. (2017). Machine learning algorithms for modeling groundwater level changes in agricultural regions of the U.S. *Water Resources Research, 53*, 3878–3895.

Semenov, M. A., & Stratonovitch, P. (2015). Adapting wheat ideotypes for climate change: accounting for uncertainties in CMIP5 climate projections. *Climate Research, 65*, 123–139.

Sheffield, J., Goteti, G., & Wood, E. F. (2006). Development of a 50-year high-resolution global dataset of meteorological forcings for land surface modeling. *Journal of Climate, 19*(13), 3088–3111.

Smiatek, G., Kaspar, S., & Kunstmann, H. (2013). Hydrological climate change impact analysis for the Figeh spring near Damascus, Syria. *Journal of Hydrometeorology, 14*(2), 577–593.

Sun, Y., Wendi, D., Kim, D. E., & Liong, S. Y. (2016). Technical note: application of artificial neural networks in groundwater level forecasting- a case study in a Singapore swamp forest. *Hydrology and Earth System Sciences, 20*, 1405–1412.

Swingler, K. (1996). *Applying neural networks: a practical guide*. Morgan Kaufmann publishing 303p.

Tapoglou, E., Trichakis, I. C., Dokou, Z., Nikolos, I. K., & Karatzas, G. P. (2014). Groundwater-level forecasting under climate change scenarios using an artificial neural network trained with particle swarm optimization. *Hydrological Sciences, 59*(6), 1225–1239.

Taylor, R. G., Scanlon, B., Döll, P., Rodell, M., Beek, R. V., Wada, Y., Longuevergne, L., LeBlanc, M., Famiglietti, J., Edmunds, M., Konikow, L., Green, T. R., Chen, J., Taniguchi, M., Birkens, M. F. P., Macdonald, A., Fan, Y., Maxwell, R. M., Yechieli, Y., Gurdak, J. J., Allen, D. M., Shamsudduha, M., Hiscock, K., Yeh, P. J. F., Holman, I., & Treidel, H. (2013). Groundwater and climate change. *Nature Climate Change, 3*(4), 322–329.

Thrasher, B., & Nemani, R. (2015). NEX-GDDP technical note version 1. Washington D. C.

Thrasher, B., Maurer, E. P., McKellar, C., & Duffy, P. B. (2012). Technical note: bias correcting climate model simulated daily temperature extremes with quantile mapping. *Hydrology and Earth System Sciences, 16*, 3309–3314.

Toth, E., Brath, A., & Montanari, A. (2000). Comparison of short-term rainfall prediction models for real-time flood forecasting. *Journal of Hydrology, 239*(1–4), 132–147.

Trichakis, I. C., Nikolos, I. K., & Karatzas, G. P. (2011). Artificial neural network (ANN) based modeling for karstic groundwater level simulation. *Water Resources Management, 25*(4), 1143–1152.

Trotochaud, J., Flanagan, D. C., & Engel, B. A. (2016). A simple technique for obtaining future climate data inputs for natural resource models. *Applied Engineering in Agriculture, 32*, 371–381.

Tsanis, I. K., Coulibaly, P., & Daliakopoulos, I. N. (2008). Improving groundwater level forecasting with a feedforward neural network and linearly regressed projected precipitation. *Journal of Hydroinformatics, 10*(4), 317–330.

Uddameri, V. (2007). Using statistical and artificial neural network models to forecast potentiometric levels at a deep well in South Texas. *Environmental Geology, 51*(6), 885–895.

Wilby, R. L., & Wigley, T. (1997). Downscaling general circulation model output: a review of methods and limitations. *Progress in Physical Geography, 21*, 530–548.

Wilby, R. L., Troni, J., Biot, Y., Tedd, L., Hewitson, B. C., Smith, D. M., & Sutton, R. T. (2009). A review of climate risk information for adaptation and development planning. *International Journal of Climatology: A Journal of the Royal Meteorological Society, 29*, 1193–1215.

Wood, A. W., Maurer, E. P., Kumar, A., & Lettenmaier, D. P. (2002). Long-range experimental hydrologic forecasting for the eastern United States. *Journal of Geophysical Research,* 107 (D20).

Wood, A. W., Leung, L. R., Sridhar, V., & Lettenmaier, D. P. (2004). Hydrologic implications of dynamical and statistical approaches to downscaling climate model outputs. *Climatic Change*, 15, 189–216.

Yoon, H., Hyun, Y., Ha, K., Lee, K., & Kim, G. (2016). A method to improve the stability and accuracy of ANN-and SVM-based time series models for longterm groundwater level predictions. *Computers and Geosciences*. https://doi.org/10.1016/j.cageo.2016.03.002.